Wool Keratin Mineralization and Functionalization: Silver Nanoparticles Synthesis and Rare Earth Elements Binding

Zhixing Lin

A thesis

submitted in partial fulfillment of the

requirements for the degree of

Master of Science

University of Washington

2023

Committee:

Shuai Zhang

Francois Baneyx

Chenyang Shi

Program Authorized to Offer Degree:

Materials Science and Engineering

University of Washington

Abstract

Wool Keratin Mineralization and Functionalization:
Silver Nanoparticles Synthesis and Rare Earth Elements Binding

Zhixing Lin

Chair of the Supervisory Committee:

Shuai Zhang

Department of Materials Science and Engineering

This paper reports a facile synthesis approach of wool keratin (WK) -templated ultrasmall(≈2nm) Ag nanoparticles. WK molecules are introduced as the template protein because of the high content of the thiol group (−SH) and unique macro molecular network structure. The optimal conditions for the formation of luminescent WK@AgNPs is established by several controlled experiments. TEM, AFM, and Photoluminescent (PL) are used for investigation of morphology and confirmation of wool keratin functionality. The structure of WK@AgNPs can be clearly observed that one or more AgNPs are bridged by keratin chain to form high molecular weight species. Take a step futher, the success of silver nanoparticle synthesis provides us with an idea to make use of the thiol group for the functionalization of wool keratin. By linking the group HOPO-Malamide to the thiol group in the WK, it is possible to apply this modified WK for rare earth recovery. The CD, FTIR and XPS results confirmed that the success of modification. But the efficiency of recovery of rare earth elements need to be further studied.

TABLE OF CONTENTS

ACKNOWLEDGEMENTS

I would like to express my sincere appreciation to my supervisor Dr. Shuai Zhang, without whom I would not have been able to complete this research, and without whom I would not have made it through my masters degree! His guidance in atomic force microscope and some suggestions on my projects played a crucial role in my master's career. And special thanks to Dr. Chenyang Shi, whose insight and knowledge into the subject matter steered me through this research. I also want to thank Dr Jinrong Ma and Mr Yifeng Cai for teaching me how to test thiol group concentration with Ellman's reagent, and allow me to use the facilities in their lab, Mr. Wenhao Zhou and Haoyu Wang for helping me with TEM imaging, Mr. Kacper Lachowski for helping me with USAXS testing and Ms.Mary Nguyen for HOPO-MA synthesis. At last, I am really thankful to the CSSAS for providing a incorporative platform to communicate and collaborate with different outstanding researchers. Part of this work was conducted at the Molecular Analysis Facility, a National Nanotechnology Coordinated Infrastructure (NNCI) site at the University of Washington, which is supported in part by funds from the National Science Foundation (awards NNCI-2025489, NNCI-1542101), the Molecular Engineering & Sciences Institute, and the Clean Energy Institute.

Chapter 1. INTRODUCTION

1.1 Introduction to Keratin

Keratin is a structural fibrous protein, also known as sclerosing protein, which is the major component of the cuticle of human and animal skin and is found in exoskeleton materials such as horns, hooves, hair, feathers, and nails. Every year, more than 5 million tons of keratin-based waste are mainly disposed of from the textile industry worldwide since it is inefficient to burn it[1,2]. Sufficient quantities, biodegradability, and biocompatibility make keratin a very economical and environmentally friendly biomaterial. Keratin-based biomaterials have been widely produced and used in various biomedical applications[3]. Different products such as keratin films, hydrogels, and composite can be generated from keratin. Additional plasticizers, cross-linker, and the incorporation of other synthetic or natural polymers can change the mechanical properties of these products.

In order to gain a further understanding to have further application, we should understand the structure, chemical and mechanical properties of keratin. Keratin can be divided into hard keratin and soft keratin according to their structure, function and regulation, and particularly sulfur content, with hard keratin usually containing more sulfur. Alpha-keratin (α-keratin) is the softer form found in all vertebrates, and the beta-keratin is the harder form found only in sauropods (reptiles and birds). While α-keratin preferentially form loosely-packed bundles of cytoplasmic intermediate filaments and endow mechanical resilience to epithelial cells, β-keratin form ordered arrays of intermediate filaments embedded in a matrix of cystinerich proteins and contribute to the tough structure of epidermal appendages[4−6]. Keratin has high contents of

cystine, glycine, proline and serine, but it is low in lysine, histidine and methionine, and tryptophan is barely present[7]. Due to the disulfide bond between cysteine amino acid residues, keratin has high stability and low solubility. However, hydrogen, hydrophobic and ionic bonds also play an influential role in the stability and properties of the keratin. In this work, keratin is obtained from wool fibre. Wool keratin, which has 4–8 wt% sulfur, is known as hard keratin, and it can be classified into four different groups based on different molecular weight: the low sulphur content keratins (LS) that have a molecular weight between 45 and 60 kDa; the high sulphur content keratins (HS) with a molecular weight of between 11 and 28 kDa and the high-glycine and tyrosine content proteins with a molecular weight of between 9 and 12 kDa[8].

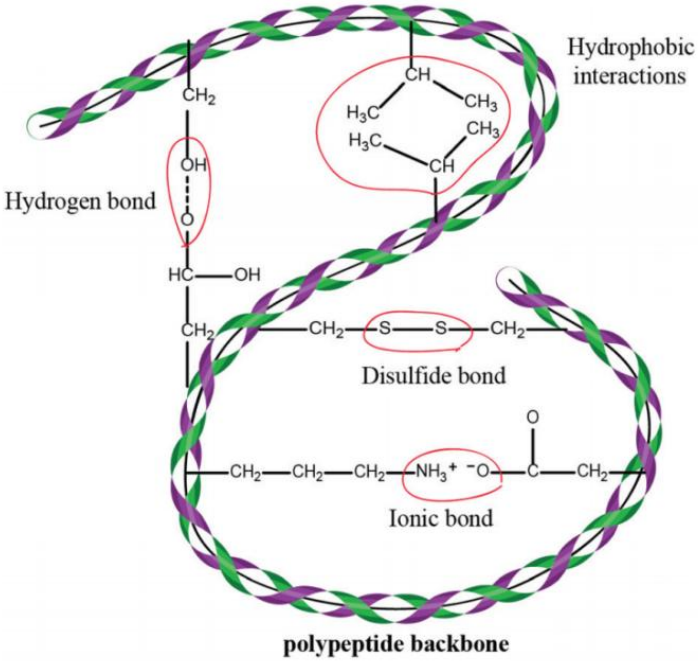

Fig.1. A diagram showing inter- and intra-molecular bonding in keratin. Various chemical bonds, e.g. hydrogen, ionic and disulfide bonds, which result in increased strength and stability of the protein, determine the structure of the keratin. [3]

Several methods are available for extracting keratin from natural resources. Six methods are commonly used for keratin extraction from wool, which are presented in previous literature. Keratin can be extracted from wool by cleavage of the disulfide and hydrogen inter-chain bonds with reducing agents, such as thiols, to form cysteine (RSH), or by sulfitolysis with sodium sulfite to form cysteine (RSH) and cysteine-Ssulfonate ($RSSO_3H$) or using oxidizing agents, such as peracetic acid, to form sulfonic acid (RSO_3H)[9].

In this work, thiol groups work as one of the reducing agents for AgNP synthesis. Non-natural wool keratin is constituted by wool keratin and HOPO binding units for the selective bioabsorption of lanthanides. Thiol groups in the wool keratin are used as attachment points for the HOPO moieties. Therefore, considering the high concentration of thiol group is required for mineralization and functionalization, the sulfitolysis method is applied for keratin extraction.

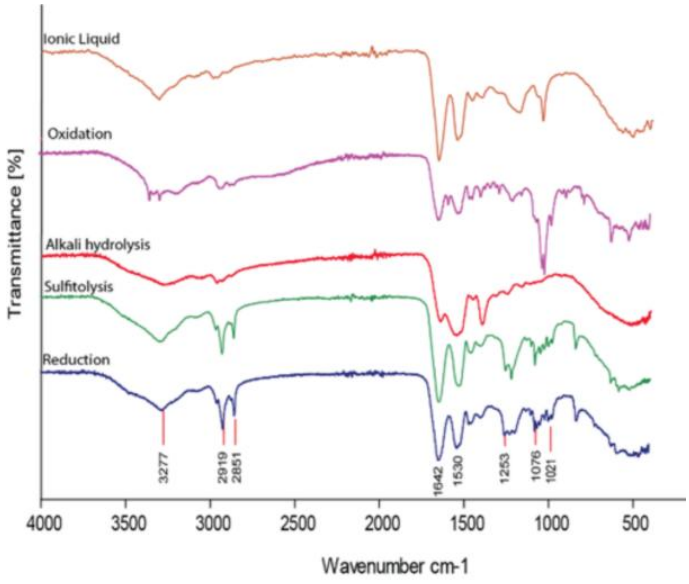

Fig.2. FTIR spectra of keratin samples (R: reduction; S: sulfitolysis; O: oxidation; IL: ionic liquid; and A: alkali hydrolysis).[9]

1.2 PROTEIN-TEMPLATED NANOPARTICLES

In recent years, photoluminescent noble metal nanoparticles with a core size smaller than 2 nm have gained attention as a promising alternative to conventional photosensitizers. [10,11]These nanoparticles exhibit superior properties, which include discrete and size-dependent electronic structures[12], intense photoluminescence (PL)[13], magnetism[14], intrinsic chirality[15], and high catalytic activity[16]. These unique properties make them ideal for bridging the research gap between isolated atoms and crystalline metal nanoparticles (NPs) (with a core size >2 nm).

Since the first report of bovine serum albumin (BSA)-templated Au nanoparticles in 2009[17], a broad variety of proteins, including BSA and human serum albumin (HSA)[18], horseradish peroxidase[19], and many more, have been demonstrated to synthesize luminescent Au nanoparticles. The resultant protein-templated Au nanoparticles have shown versatile biological applications such as sensing, cellular imaging, tumor site targeting, intercellular pH indication, and drug screening[10].

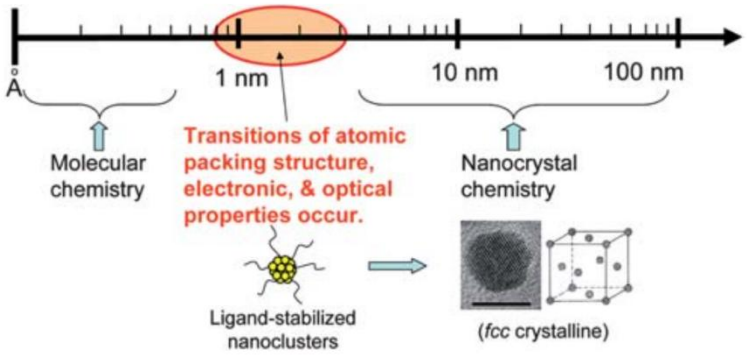

Fig.3. Metal nanoclusters, bridge organometallic complexes andnanocrystals.[10]

Compared to the extensive investigations of protein-templated Au nanoclusters documented in the scientific literature, the synthesis and application of their Ag counterparts are surprisingly scarce. One of the potential reasons for this disparity in exploration is that the reduction of Ag^{+} to its metallic state is more challenging than that of Au^{3+}, as the redox potential of Ag^{+}/Ag (approximately 0.8 V) is lower than that of $AuCl_4^{-}/Au$ (approximately 1.0 V). The commonly utilized reducing agents for the synthesis of Au nanoclusters, such as tyrosine [17] residues present in BSA, are thus insufficiently potent to reduce Ag^{+}; consequently, stronger extrinsic reducing agents, such as $NaBH_4$, are required, which further increase the complexity of the reaction system. Furthermore, Ag nanoparticles exhibit lower stability compared to Au nanoparticles and are more susceptible to their environment. The presence of atmospheric oxygen during their synthesis can intensify the challenge of reproducing Ag nanoparticles, as it can trigger oxidative decomposition. Therefore, the development of more durable and dependable synthesis methods for protein-templated Ag nanoparticles is urgently needed to investigate their largely unexplored properties and potential practical applications.

Chemical reduction of silver salts is a commonly utilized technique to fabricate Ag nanoparticles[20]. Chemical reduction is simple and facile compared to other methods used in synthesizing silver nanoparticles, including chemical, electrochemical, and thermal reduction methods. However, these freshly reduced nanoparticles tend to be highly unstable and predisposed to aggregate into larger structures. The nanoparticles need to be safeguarded against aggregation to maintain their excellent properties. A variety of surfactants, polymers, dendrimers, biological templates, and biomacromolecules can be employed to protect the nanoparticles[21-24]. In the investigations conducted by Raveendran et al.[25], b-D-glucose served as the reducing agent, while starch played the role of stabilizer. In another study, Ag NPs were

generated using acacia, which functioned effectively as both reducing and stabilizing reagents [26]. An emerging area of focus in nanotechnology is the application of nanoparticles in biology. Microorganisms, including bacteria, fungi, and spent mushroom substrate, as well as DNA and proteins, have been reported as effective tools in the synthesis of Ag nanoparticles via their strong affinity to silver with –SH, –NH2, and –COOH ligands [27-29]. In these investigations, the size of the Ag nanoparitcles can be regulated by adjusting different parameters such as pH, temperature, substrate concentration, and reaction time.

Keratin, an insoluble fibrous protein, serves as the primary constituent of various epithelial coverings such as wool, feathers, nails, and horns. In comparison to alternative capping agents, employing keratin to coat nanoparticles affords several advantages. Firstly, keratin ranks among the most abundant proteins available, with a keratin content of over 50 weight percent present in both wool and feathers [30]. This high content translates into lower extraction and purification costs when compared to other proteins. Secondly, given the elevated concentration of cysteine residues relative to other proteins, keratin represents an optimal choice for stabilizing heavy metal nanoparticles. Thirdly, Different products such as keratin films, hydrogels, and composite can be generated from keratin. Additional of plasticizers, cross linker and incorporation of other synthetic or natural polymer can change the mechanical properties of these products. Finally, due to their biocompatibility and biodegradability, nanoparticles coated with keratin can be seamlessly integrated into systems relevant to pharmaceutical and biomedical pursuits.

1.3 Recovery of Rare Earth Elements

Rare earth elements (REEs), which are also called rare-earth metals or, in context, rare-earth oxides, encompass the lanthanides, yttrium, and scandium, representing indispensable resources for transitioning from the era of fossil fuels into the low-carbon era. Among these elements, five REEs (Tb, Dy, Eu,Nd, and Y) have been identified by the U.S. Department of Energy as exhibiting high supply vulnerability and criticality with regard to clean energy technologies, including electric vehicles, wind turbines, and LEDs. Nonetheless, the present methods of REE extraction and separation consume significant energy and engender grave environmental concerns that threaten to stifle the emergence of a diversified REE supply chain while diminishing the environmental advantages associated with clean energy technologies. To satisfy the growing demand for REEs within the clean energy technology market, it is thus of utmost importance to develop new processing techniques that enable the environmentally sustainable extraction of REEs from current and future sources.

REEs represent fundamental raw materials in a diverse array of applications, including metallurgy (metal refining and metal alloying), catalysis in the automotive and petrochemical industries, colouring of glass and ceramics, phosphors (LEDs, compact fluorescent lamps, flat panel displays), lasers, rechargeable solid-state batteries (Ni-MH), fiber optics, and other fields.[31]Moreover, REEs play an indispensable role in emerging technologies such as solid-state fuel cells, superconductors, magnetic cooling, hydrogen storage, and high-performance permanent magnets. The latter are of particular importance in a wide range of cutting-edge applications, ranging from wind turbines and hybrid cars to HD drives, cell phone speakers, and microphones.

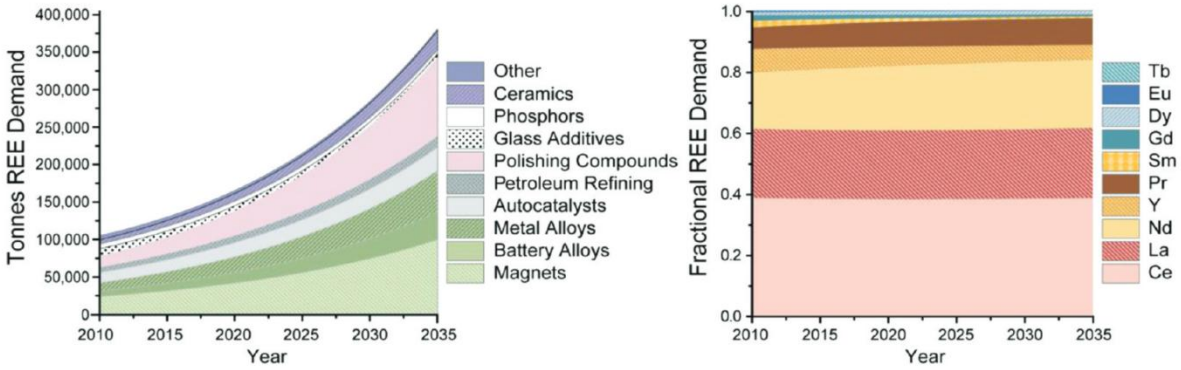

Fig.4. Evolution of market distribution of REE demand: Totals (left) and individual REE market share (right). Average annual growth between 2010 and 2035 is 5.3%[31]

The demand for rare-earth elements (REEs) has been steadily increasing due to their expanding range of uses and applications over the years. Therefore, it has become crucial to recover REEs from waste streams or the aqueous solution obtained during hydrometallurgy. There are several conventional techniques used for the recovery of REEs, including precipitation, electrocoagulation, flotation, solvent extraction (SE), ion exchange, and adsorption. However, these methods have their limitations.

Precipitation is commonly used to recover REEs from wastewater, but it is not a feasible process for effluents with low REE concentrations due to the high volumes of chemicals required and sludge generated. Electrocoagulation is highly efficient but has a high operational cost, and the short life cycle of the used anode is a significant drawback. Flotation is cost-effective, but a post-treatment process is required to achieve REEs with the desired purity.

Given the increasing demand for REEs in emerging clean energy technologies, there is an urgent need to develop new and more efficient approaches for their extraction and recovery. The development of such approaches would enable the recovery of REEs from low-grade and complex feedstocks, which would otherwise be challenging to extract using conventional

techniques. Such innovative approaches would provide significant benefits, including reduced environmental impact, improved sustainability, and enhanced economic viability of REE recovery processes. Therefore, research efforts are being directed towards developing new technologies that can effectively recover REEs from complex waste streams while minimizing environmental impact and maximizing economic efficiency. These technologies include bioleaching, membrane separation, and magnetic separation, among others. With the continued exploration of these and other innovative techniques, the efficient extraction and recovery of REEs could become a reality, meeting the growing demand for these critical elements

The use of biological ligands in solid-liquid extraction processes has shown potential for novel chemistries and environmentally sustainable REE separation process development. Lanmodulin (LanM) is a small protein involved in lanthanide trafficking in methylotrophic bacteria and has shown promise as a new ligand for process development[32]. Recent biochemical and biophysical characterization of LanM has revealed remarkable selectivity for REEs against non-REE cations, the ability to bind REEs down to pH≈2.5, and uncommon robustness to repeated acid treatment cycles. Another commonly used biological ligand for REEs recovery is lanthanide binding tags (LBTs). LBTs are short peptides engineered for affinity and selectivity toward REEs, displayed on biomaterial surfaces, and employed in solid-liquid extraction for selective recovery of middle and heavy REEs from various feedstock leachates. However, the low selectivity against Cu2+ and negligible REE binding below a pH of 5 limits the feedstock compatibility of LBTs[33].

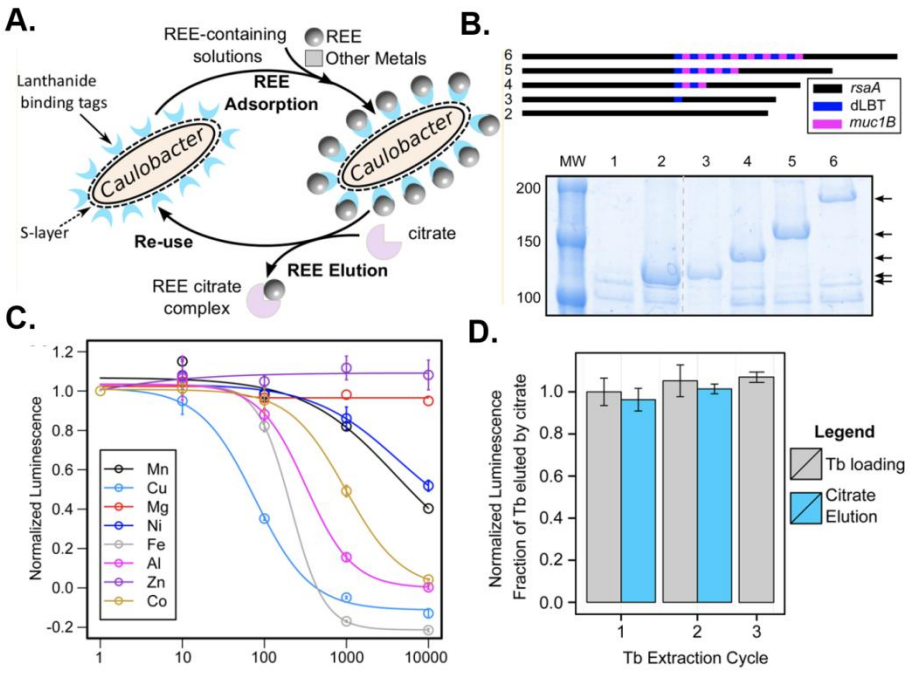

Fig.5. (A) Scheme of using LBTs for REEs recovery cycle(B)Diagram of engineered S-layer gene (rsaA) constructs with dLBT insertions. (C)Competition binding experiments with dLBTx4 cells preloaded with 10μM Tb3+ followed by addition of various metal ions at concentrations up to 10 mM.(D)No reduction in Tb3+ adsorption capacity was observed following citrate elution, enabling consecutive adsorption/desorption cycles.

While natural lanthanide-binding proteins and designed de novo proteins can display extremely high binding affinities for f-elements, their applications for large-scale extraction or the separation of each lanthanide from one another are expected to be challenging. Therefore, strategies that exploit more readily accessible and tunable bioinspired materials would be highly beneficial for the recovery and purification of rare-earth elements. In conclusion, the incorporation of wool keratin and HOPO-MA group for REEs recovery offers a potential solution to overcome the challenges of current ligand-based methods.

Chapter 2. EXPERIMENT METHODS

2.1 MATERIAL PREPARATION

2.1.1 *Materials*

Disodium sulfide(Na_2S), Sodium Dodecyl Sulfate (SDS), Sodium borohydride (NaBH4) , silver nitrate (AgNO3), europium (III) chloride hexahydrate 99.99%, 2-(Nmorpholino)ethanesulfonic acid (MES), N-2-hydroxyethylpiperazine-N'-2-ethanesulfonic acid (HEPES), were purchased from Sigma-Aldrich (St. Louis. MO, USA). All solutions were preparedwith Milli-Q water with a specific resistance of 18.2 MΩ.

2.1.2 *Wool Keratin Extraction and Ellman's Assay*

Fig.6. Schematic of wool keratin extraction process

Wool keratin solutions were extracted from wool by reducing disulfide bonds with Na2S. Briefly, the wool fibers were cleaned by immersing them in DI water for 2 hours to remove impurities and grease from the surface. Then, 5 g of the scoured wool fibers were dispersed in 100 ml of an aqueous solution containing 8 M urea, 0.1 M SDS, and 0.1 M Na2S, and the

mixture was incubated at 50 °C for 16 h. The resulting solution was filtered to remove impurities and denaturants, and the protein was then subjected to dialysis for at least 3 days, with frequent changes of deionized water, using a dialysis cassette with a molecular weight cutoff of 3500. Two different keratin solutions were obtained, depending on the concentration of Na2S used (0.1 M or 0.2 M). The resulting protein samples were then frozen with liquid nitrogen and lyophilized in a freeze-dryer. The resulting powders were stored at -20 °C until use.

The thiol group concentration was measured by using Ellman's assay.

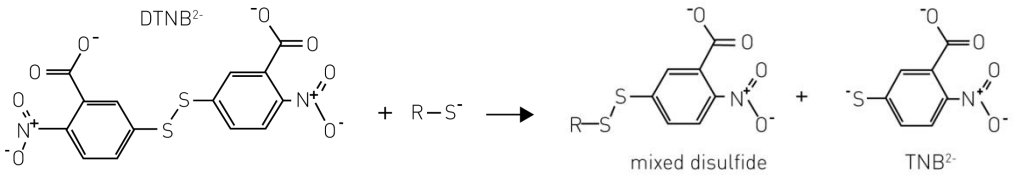

Fig.7.Reduction of Ellman's reagent

In this experiment, a Flat-Bottom 96-well plate and a BioTek Synergy LX Multi-Mode Microplate Reader (FLD/Lumi) are used to determine the concentration of cysteine in the WK solution. The reaction buffer (RB) used in this experiment is 0.1 M sodium phosphate, pH 8.0, containing 1 mM EDTA. Cysteine Hydrochloride Monohydrate (MW 175.6) and Ellman's Reagent 5,5-dithio-bis-(2-nitrobenzoic acid) are also used. Firstly, the solutions of Ellman's Reagent and cysteine hydrochloride are prepared at room temperature prior to use. The Ellman's Reagent Solution is prepared by dissolving 4 mg of the thawed Ellman's Reagent in 1 mL RB. Next, Standard A (1.6 mM) is prepared by dissolving cysteine hydrochloride in RB. A set of cysteine standards is then prepared by diluting Standard A in a 2-fold dilution series to 0.1 mM. Two different concentrations of WK(20mg/ml, 10mg/ml) are also prepared. Test tubes are then set up, each containing 25 µL of Ellman's Reagent Solution and 1.25 mL of RB. 125 µL of each

standard or unknown is added to separate test tubes. The solutions are mixed and incubated at room temperature for 15 minutes. Finally, 200 µL of each solution is added to a 96-well plate, and the full absorbance spectrum of the compound is determined using the BioTek Synergy LX Multi-Mode Microplate Reader (FLD/Lumi).

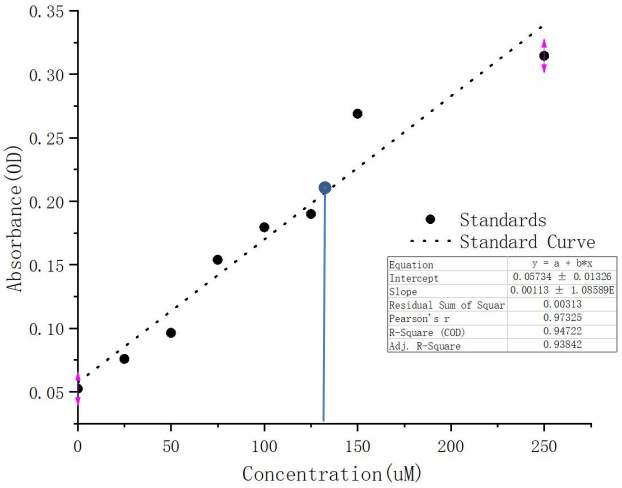

Fig.8. Quantification of free thiol groups in WK1. The blue dot represents the absorbance value of WK1 solution at concentration of 20mg/ml.

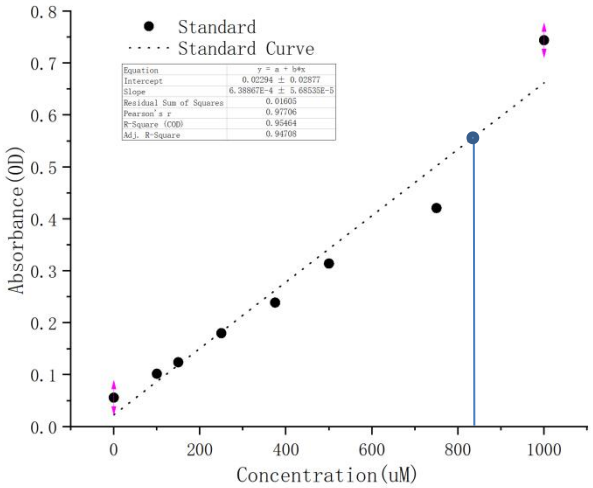

Fig.9.Quantification of free thiol groups in WK2. The blue dot represents the absorbance value of WK2 solution at concentration of 20mg/ml.

The standard curves are generated by plotting each value obtained 412nm for the standards. The thiol group concentrations of different kinds of wool keratin from these curves are then determined by using the following formula:

$$C_{sulfhydryls} = \frac{Absorbance\ of\ WK\ solution - Y\ value\ of\ Std.Curve}{Slope\ of\ Std.Curve}$$

By applying this formula, the free thiol group concentration in two different wool keratin solution can be easily calculated. The results of WK1 and WK2 are shown as Table 1.

Keratin Type	Na_2S	Free thiol group content
WK1	0.1M	128uM
WK2	0.2M	812uM

Table.1. Free thiol group concentration of WK1 and WK2

2.1.3 *Wool keratin-templated silver nanoparticles synthesis*

First, to prepare the WK@AgNPs, 50 mg of WK were dissolved in 5 mL of deionized (DI) water. While placing the sample on the cimarec stirring hot plate and stirring with the magnetic stir bar at room temperature (RT), 5 mL of 10 mM silver nitrate ($AgNO_3$) solution was gradually added drop by drop to the WK solution and incubated for 5 minutes at RT. Following the incubation, 0.5 mL of 1 M NaOH was introduced to the WK-Ag complex. After another 5-minute incubation period, 0.5 mL of $NaBH_4$ (10 mM) solution dissolved in NaOH (0.1 M) was

added to the solution to form the WK@AgNPs. The final WK@AgNPs samples were refrigerated at 4◦C until further use.

2.1.4 *Wool keratin functionalized with HOPO-MAL group*

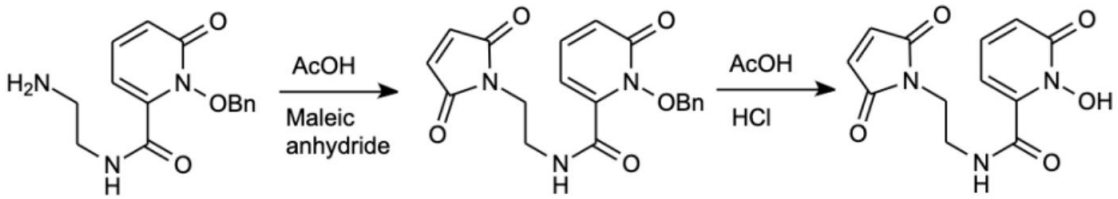

Fig.10. Schematic of HOPO-MA synthesis

The linker HOPO-MAL was synthesized based on the process illustrated in previous literature[33]. The first step of synthesis was dissolving 200 mg of the precursor in 3 mL of glacial acetic acid (AcOH). Subsequently, 117 g of maleic anhydride was added to the mixture, and the reaction was carried out at 125 °C for 5 hours. The resulting mixture was then subjected to reduced pressure to remove any volatiles, and 55 mL of saturated NaHCO3 was added to neutralize the acetic acid. The organic phase was extracted from the aqueous phase using AcOEt (25 mL in total), resulting in a yellow and transparent solution. The organic phase was then washed twice with 1 M HCl and once with brine, followed by drying with MgSO4. The solvent was evaporated under reduced pressure to yield 100 mg of the product, which was then dissolved in 5 mL of glacial acetic acid. 5 mL of HCl (37%) was added to the solution, which was left to react and stir for 48 hours at room temperature. The final product was obtained through vacuum isolation.

40mg of WK powder were dissolved in 200 mL HEPES buffer (20 mM) at pH 7.3. 1 mL DMSO containing HOPO-maleimide(20mM) were added to the solution, and the resulting

sample was mixed vigorously, and left shaking at room temperature for 12h. The protein suspension was washed three times (8000 rpm × 5 min) to eliminate unbound HOPO-maleimide and residual DMSO, and the protein flakes were finally resuspended in MES buffer (0.375 M, pH 6.0) before capturing Eu^{3+}.

Buffering of the solution was assured by the addition of HEPES and MES buffers (10 mM).

2.2 CHRACTERIZATION

2.2.1 *Microscopy(TEM/AFM)*

The samples were examined using a transmission electron microscope (FEI, Sam Tecnai F20 SuperTwin) at 200kV, and the resulting electron micrographs were recorded with a CCD camera and Gatan Digital Micrograph software. The particle size distribution and transmission electron microscopy image analysis were conducted using ImageJ software. The negative staining procedure was carried out on wool keratin samples at a concentration of 2mg/ml, using carbon-coated 200 mesh copper grids. Specifically, 10 uL of the sample solution was applied to the grids, which were then incubated for 5 minutes at room temperature. After incubation, excess protein solution was removed by blotting the grids with filter paper. Subsequently, 5 uL of TPA was added to the grids, and after waiting for another 5 minutes, the excess stain was removed with filter paper. Finally, the grids were air-dried before imaging.

For ex-situ atomic force microscope (AFM) imaging, Bruker Dimension ICON AFM (Bruker, Billerica, MA) was used in PeakForce Tapping mode in air. Image analysis was conducted using Gwyddion software.

2.2.2 *Photoluminesent (PL)*

Emission spectra were recorded on a Perkin Elmer LS-55 Luminescence Spectrophotometer with pulsed high pressure Xenon source. All photophysical properties were measured in buffered aqueous solutions at pH 7.4. The excitation slit widths were routinely set at 10nm and the emission slit widths were set at 5nm.

2.2.3 *XPS*

All XPS spectra were taken on a Kratos Axis-Ultra DLD spectrometer. This instrument has a monochromatized Al Kα X-ray and a low energy electron flood gun for charge neutralization. X-ray spot size for these acquisitions was on the order of 700 x 300 μm. Pressure in the analytical chamber during spectral acquisition was less than 5 x 10-9 Torr. Pass energy for survey and detailed spectra (composition) was 80 eV. Pass energy for the high resolution spectra was 20 eV. The take-off angle (the angle between the sample normal and the input axis of the energy analyzer) was 0 degree(0 degree take-off angle ~ 100 Å sampling depth). The Kratos Vision2 software program was used to determine peak areas and to calculate the elemental compositions from peak areas. CasaXPS was used to peak fit the high resolution spectra. For the high-resolution spectra, a Shirley background was used and all binding energies were referenced to the C ls C-C bonds at 285.0 eV.

Chapter 3. RESULTS AND DISCUSSION

3.1 WOOL KERATIN-TEMPLATED SILVER NANOPARTICLES

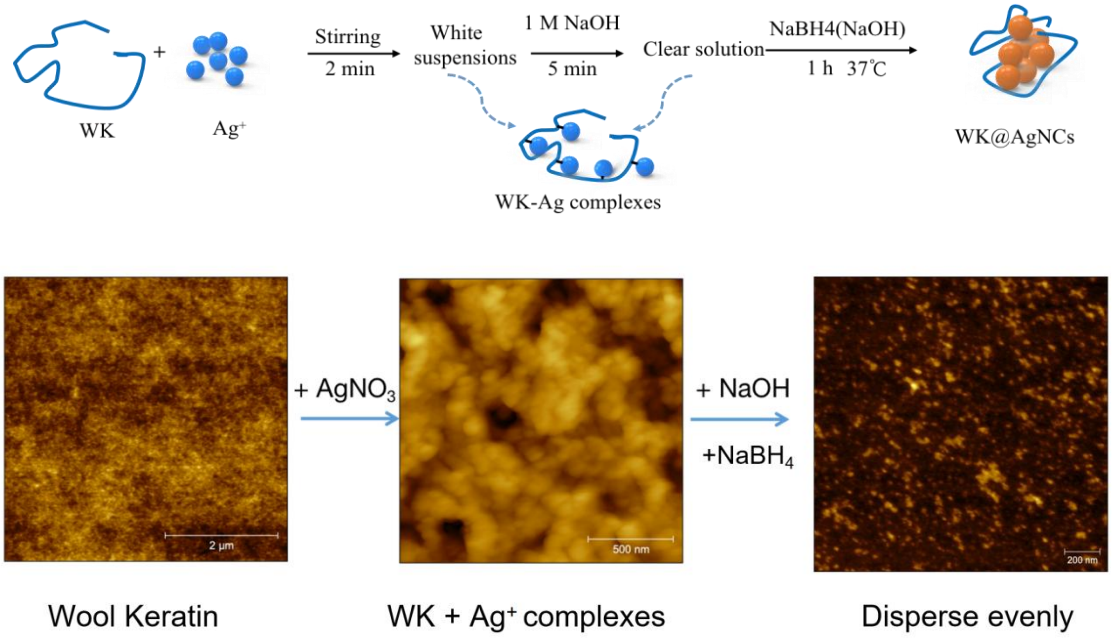

Fig.11. (A)Schem of WK@AgNPs synthesis;(B)Ex situ AFM images of each synthesis step

Figure 11(A) displays the schematic of wool keratin-templated AgNPs synthesis. In a typical protocol, aqueous solutions of wool keratin (WK) and $AgNO_3$ were initially blended to create a white suspension as a result of the coordination between Ag ions and the numerous functional groups present in WK (e.g., NH_2, OH, and SH), forming insoluble complexes. A small amount of NaOH was added 2 minutes later to dissolve the insoluble complexes and adjust the solution's pH to 12. Nonetheless, thiol groups lack sufficient reductant capabilities to reduce Ag^+ to Ag^0. Consequently, a $NaBH_4$ solution dissolved in NaOH (hereafter referred to as $NaBH_4$(NaOH)) was introduced to reduce the Ag ions and generate AgNPs within an hour. The

as-formed Ag NCs exhibited a reddish-brown hue in solution and a shoulder peak at around 415 nm on their absorption spectra. When exposed to UV light irradiation, they demonstrated a red emission with a photoemission peak centered at ≈605 nm.

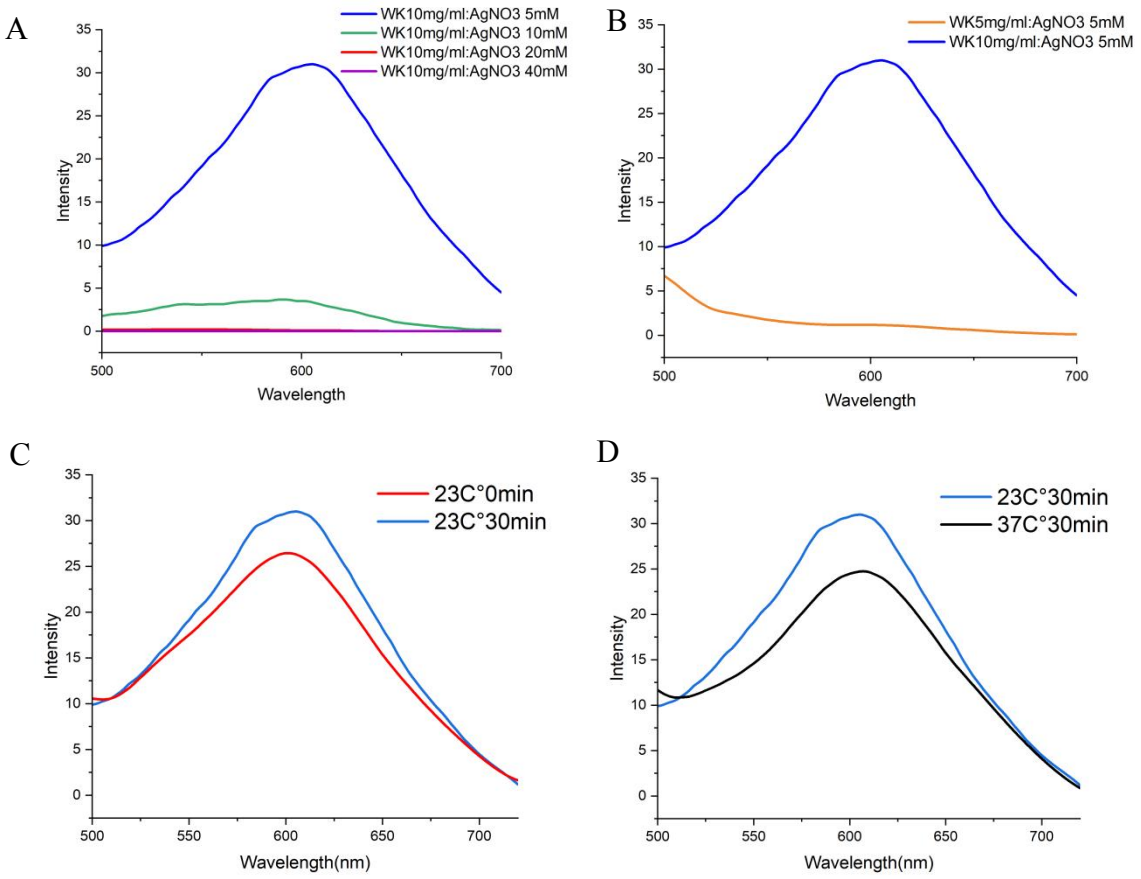

Fig.12. PL spectra of AgNPs synthesized under different conditions

(A)$AgNO_3$ concentration; (B)WK concentration; (C)incubation time; (D)incubation temperature

Several other control experiments were also carried out to establish the optimal conditions for the formation of luminescent WK@AgNPs. Initially, we standardized the wool concentration to 10mg/ml, after which we varied the concentration of $AgNO_3$ between 5mM and 40mM. Through this experimentation, we discovered that the optimal concentration for producing silver nanoparticles with the highest fluorescence intensity was at 10mM of $AgNO_3$. Subsequently, we

manipulated different concentrations of WK to acquire the silver nanoparticles with the brightest fluorescence. Our efforts led to the discovery of the optimal synthesis ratio of WK: $AgNO_3$ as 10mg/ml:5mM. Furthermore, the optimization of WK@AgNPs fluorescence can be achieved by modulating various temperature and incubation parameters. Specifically, incubating the freshly synthesized AgNPs in the incubator at a temperature of 23°C for a duration of 30 minutes results in the brightest AgNPs fluorescence.

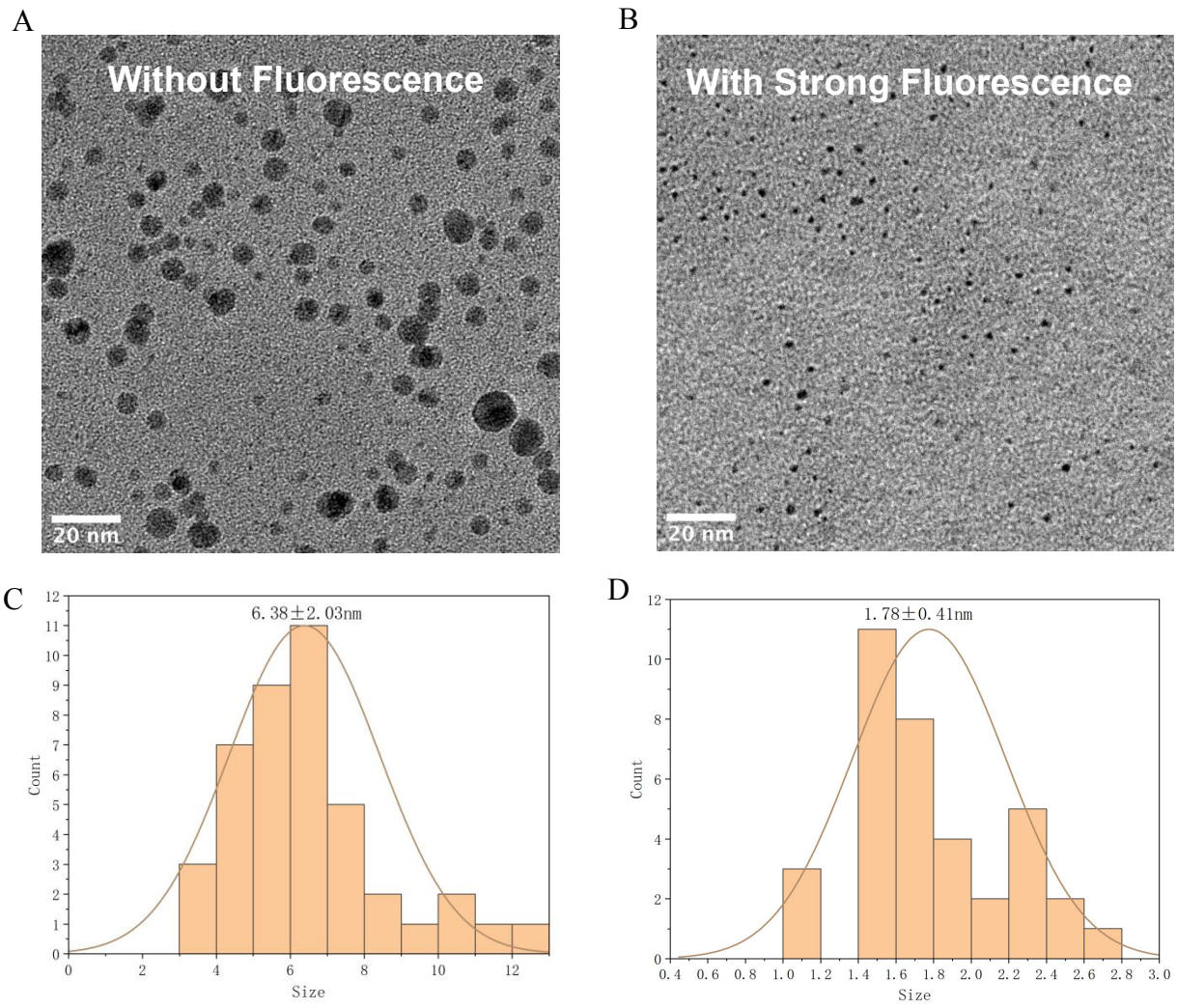

Fig.13. (A)TEM image of WK@AgNPs without fluorescence;(B)TEM image of WK@AgNPs with strongest fluorescence;(C)particle size distribution histogram of (A);(D)particle size distribution histogram of (B)

The impact of various factors, such as the concentration of WK, $AgNO_3$, and incubation temperature and duration, on the fluorescence intensity of $AgNO_3$ has been investigated. The TEM data has led to the conclusion that the fluorescence of these AgNPs is dependent on their size. Figure 13(A)(B) showcases two TEM images of the nanoparticles generated, revealing their isotropic shape with a low aspect ratio. The synthesis of Ag(0) NPs occurred through the reduction of Ag+ within the nanoscopic starch templates. A particle size distribution histogram, presented in Figure 13(C) and (D), highlights that the mean particle diameter of AgNPs without fluorescent is 6.38 nm with a standard deviation of 2.03 nm while the mean particle diameter of AgNPs with strongest fluorescent is 1.78 nm with a standard deviation of 0.41 nm. Notably, we conducted a series of controlled experiments in which we varied the concentration of thiol groups in wool while keeping the wool concentration constant. Our results revealed a positive correlation between thiol group concentration and AgNPs radius. However, when we increased the wool concentration sixfold while using the same type of WK, we observed that the resulting AgNPs had a larger particle size compared to those obtained by increasing only the thiol group concentration by sixfold. This suggests that while thiol groups in WK are the main contributors to AgNPs synthesis, other functional groups in WK also play a significant role in affecting particle size.

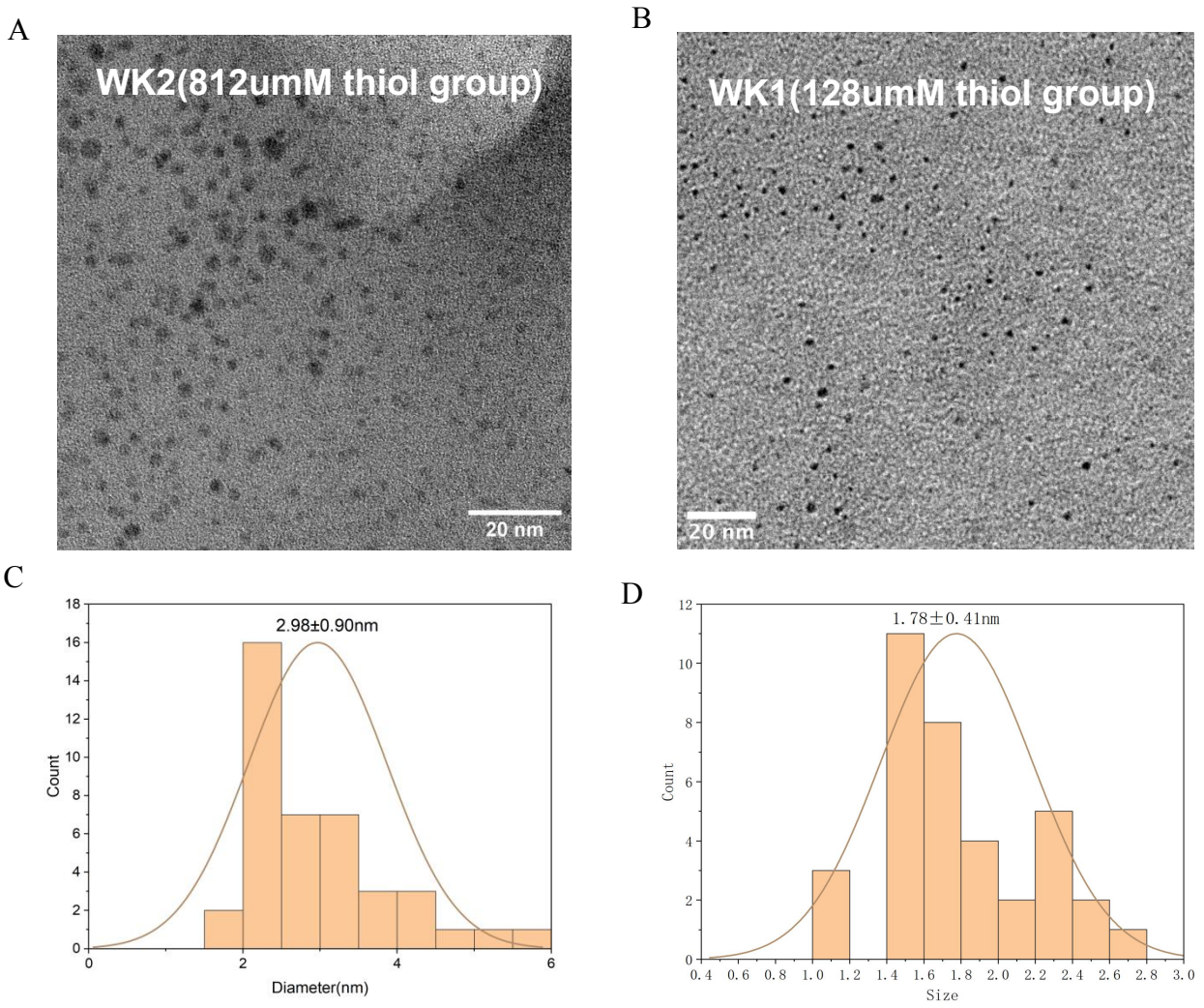

Fig.14.(A)TEM image of WK@AgNPs synthesize with 10mg/ml WK2 ;(B)TEM image of WK@AgNPs synthesize with 10mg/ml WK1;(C)particle size distribution histogram of (A);(D)particle size distribution histogram of (B)

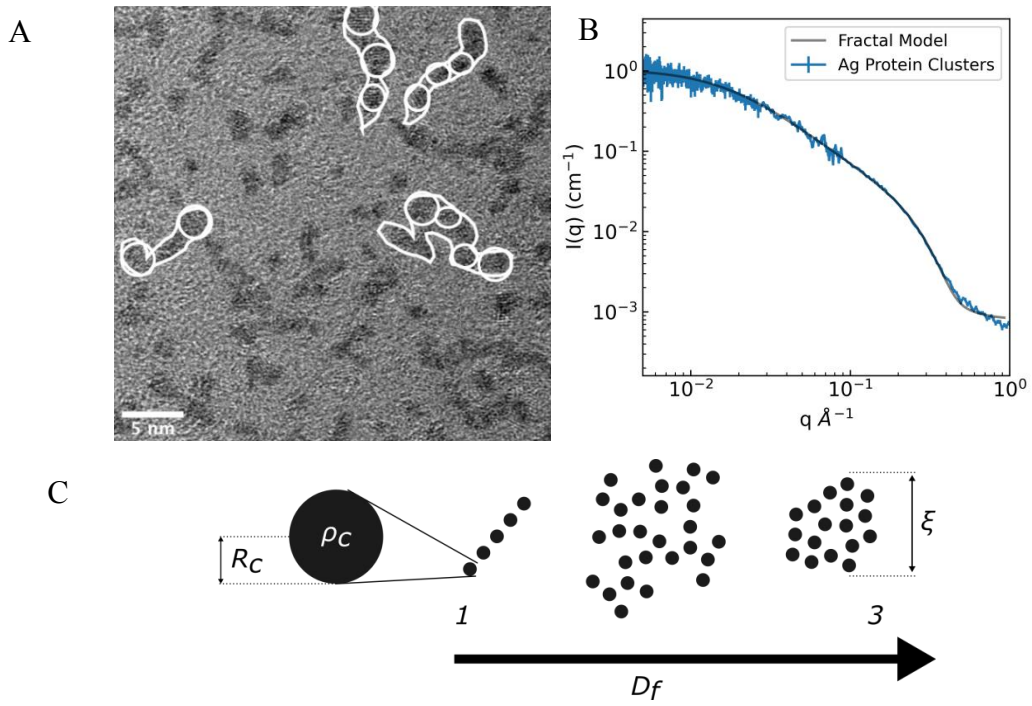

Fig.15. (A)Negative staining TEM image of WK@AgNPs;
(B) USAXS data and model fitting curve; (C)Fractal model of WK@AgNPs

Despite using transmission electron microscopy (TEM) to measure the size of WK@AgNPs and atomic force microscopy (AFM) to investigate the synthesis process of WK@AgNPs, the mechanism of wool binding to silver nanoparticles remains unknown. To shed light on this process, negative staining and ultra-small-angle X-ray scattering (USAXS) techniques are employed to build a model that explains how silver nanoparticles combine with wool keratin. Negative staining is a powerful technique in TEM that allows for the visualization of organic samples by introducing a contrasting agent around them. At the same time, USAXS is used to study the nanoscale structure of materials in solution. These complementary techniques are expected to provide insight into how wool keratin binds to silver nanoparticles, which has remained elusive despite previous studies. Using negative staining and USAXS, we hope to understand better the interactions between wool keratin and silver nanoparticles and develop a model that accurately describes this process. The model will be based on the observed structure

and behavior of the WK@AgNPs complex and the individual components' physical and chemical properties.

This USAXS model describes a fractal structure made up of 1.4 nm diameter spherical subunits that are aggregated in a diffusion-limited way, resulting in a loosely packed structure with a characteristic correlation length of 8.1 nm. The fractal dimension (Df) of the structure is 1.7, indicating a complex, rough, and porous structure. The subunits aggregate randomly in space and create voids or pores between them. The model predicts a decrease in scattered intensity with increasing q due to the fractal nature of the structure, and the scattering pattern can be described by the fractal dimension and correlation length of the structure. The curve fitted using the aforementioned model data corresponds well with the USAXS data we obtained. The size of the subunit in the model is consistent with that of the observed silver nanoparticles, while the correlation length in the model matches the size of the particles enveloped in wool observed after negative stain. This serves to further authenticate the precision of our model.

3.2 FUNTIONALIZED WOOL KERATIN FOR REES RECOVERY

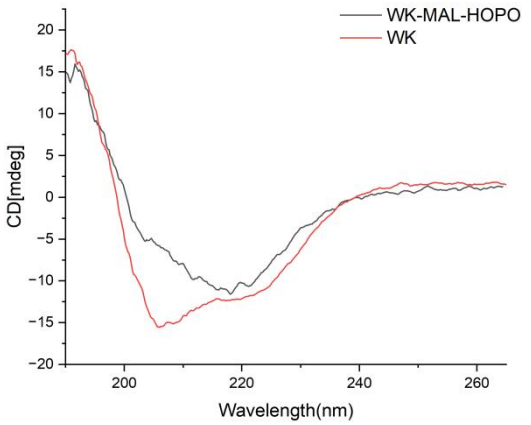

Fig.16. CD spectrum of WK and funtionalized WK

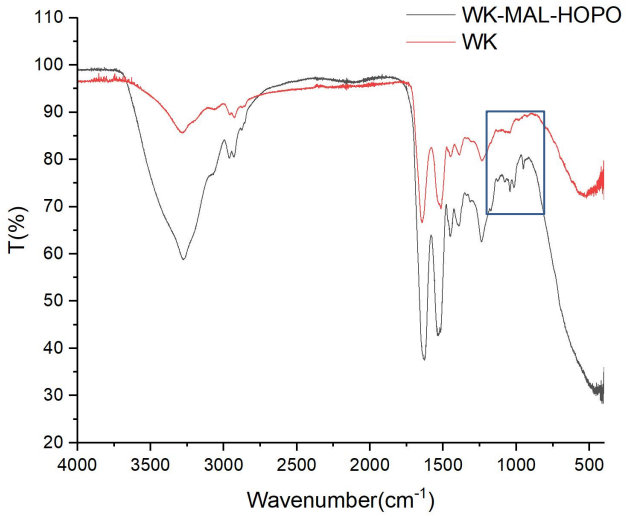

Fig.17. FTIR spectrum of WK and functionalized WK

The secondary structure of a protein can be determined using circular dichroism (CD) spectroscopy. An α-helical structure shows two negative minima of almost the same degree of ellipticity at 222 nm and 208 nm, followed by a positive maximum at 190 nm. Conversely, a negative minimum near 218 nm followed by a positive maximum at 195 nm depicts the presence of β-sheet structure. For wool keratin, the intensities of these two negative bands are not equal. There is a sharp peak showing at 208nm, and the CD spectrum also has a broad band between 200 and 235 nm, suggesting that keratin not only contain α-helical structure, but also adopts β-sheet conformation. However, functionalized wool keratin only shows a broad peak between 200-235 nm, indicating that the β-sheet structure is predominant.

The FTIR spectrum displays distinct bands that elucidate the chemical composition of a substance. The amide A band, situated at 3276 cm^{-1} according to Shavandi et al.[34], emanates from the stretching vibrations of both (N–H) and (-OH) bonds. In contrast, the amide I band, which arises from (C=O) vibrations, manifests within the range of 1600 to 1700 cm−1. The amide II band, which arises from both (N–H) deformations and stretching (C–N) vibrations,

occurs within the vicinity of 1520–1540 cm−1. Lastly, the amide III band emerges at 1220–1300 cm−1 and is due to the stretching vibrations of both (C-N) and (C–H), and bending vibrations of (N-H) and (C=O). [35,36] In the present FTIR spectrum, both unmodified WK and its functionalized counterpart exhibit a peak that has been documented in previous literature.

Aside from the typical peak that appears on the FTIR spectrum of wool keratin, there are additional peaks at 1172, 1076.25, and 1043.5 cm-1, indicating changes in the sample. However, these new peaks are located in the "fingerprint region", which is the region between 400 cm-1 and 1500 cm-1 in an IR spectrum. This region usually contains a large number of peaks, making it difficult to identify individual peaks. Nevertheless, the fingerprint region of a specific compound is unique. Therefore, these new peaks also suggest that changes have been made to our samples.

Therefore, considering the differences observed in the CD spectrum and FTIR spectrum of WK and WK-HOPO-MA, it can be partially concluded that our functionalization process was successful.

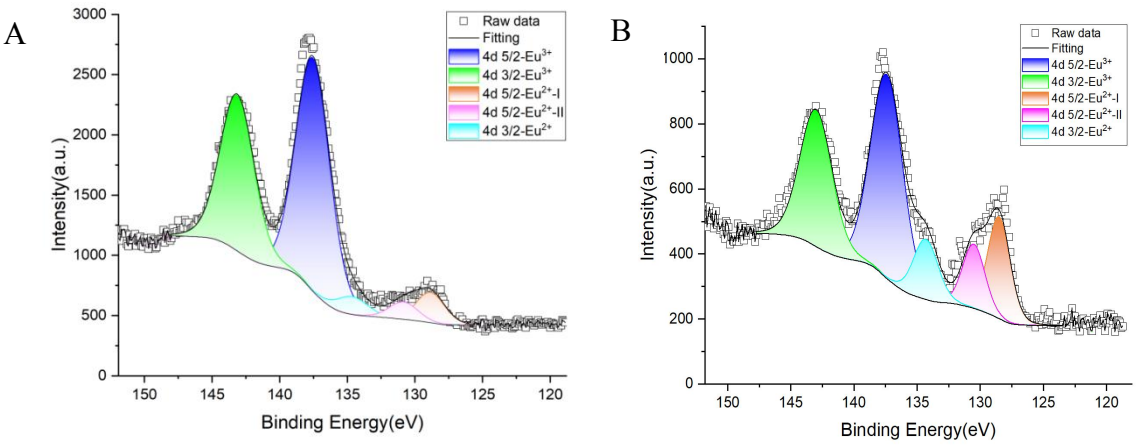

Fig.18. High resolution XPS spectra of Eu 4d.
(A)Eu^{3+} added to WK-HOPO-MA solution; (B)Eu^{3+} added to WK solution

To investigate the potential of WK and WK-HOPO-MA in capturing rare earth elements (REEs), a solution containing 160 uM of Eu^{3+} was added separately to solutions of WK and WK-HOPO-MA. Subsequently, the solutions were stirred for 1 hour, resulting in the formation of precipitate in both solutions. In order to see what these precipitate is and what happened in our solution, we pipetted the solution with precipitate on the silica flake, let these sample air dried and used XPS to identify the chemical composition of these precipitate.

Figure 13 displays a high-resolution XPS image of the Eu 4d orbital. In part A, an abundance of Eu^{3+} is apparent in the WK-HOPO-MA sample, while only a minor quantity of Eu^{2+} is present. Conversely, part B reveals a significant quantity of Eu^{2+} in the WK sample. By examining the peak areas, we estimate that the ratio of Eu^{2+} to Eu^{3+} in WK-HOPO-MA is approximately $Eu^{2+}/Eu^{3+} \approx 14.64\%$, while in the WK sample, this ratio is roughly $Eu^{2+}/Eu^{3+} \approx 48\%$.

Due to its susceptibility to reduction, Eu^{3+} is readily reduced to Eu^{2+}, and wool's SH group displays a potent reducing capacity. Consequently, a plethora of free mercapto groups within the wool sample reduces Eu^{3+} to Eu^{2+}. Moreover, wool's mercapto groups are oxidized by Eu3+, resulting in their crosslinking to form disulfide bonds, which render the wool insoluble in water. In contrast, WK-HOPO-MA has been functionalized with HOPO-MA groups, which occupy a majority of the free mercapto groups, and therefore, they lose their capacity to reduce Eu^{3+}. Additionally, HOPO-MA is hydrophobic, leading to the functionalized wool's poor solubility in water. Since HOPO-MA coordinates with Eu^{3+}, the majority of Eu in the WK-HOPO-MA sample exists in the form of Eu^{3+}.

Our hypothesis was subsequently confirmed through a series of experiments. Initially, we subjected a portion of the solution containing precipitate to dialysis using a dialysis bag for a

duration of one day. Following this, we centrifuged the precipitates from both solutions and added water to the centrifuge tubes, which were agitated vigorously for ten minutes before undergoing centrifugation once more. This process was repeated thrice to remove any unbonded Eu ions from the samples. Subsequently, we conducted XPS analysis of these samples, the results of which are presented in Figure 14. Within the XPS range of 0-1200 eV, the peak of Eu 3d BE values is detected between 1120-1145 eV, and the Eu4d BE peak appear within the XPS range of 115-150 eV. Notably, no peak of Eu was observed in the WK sample.

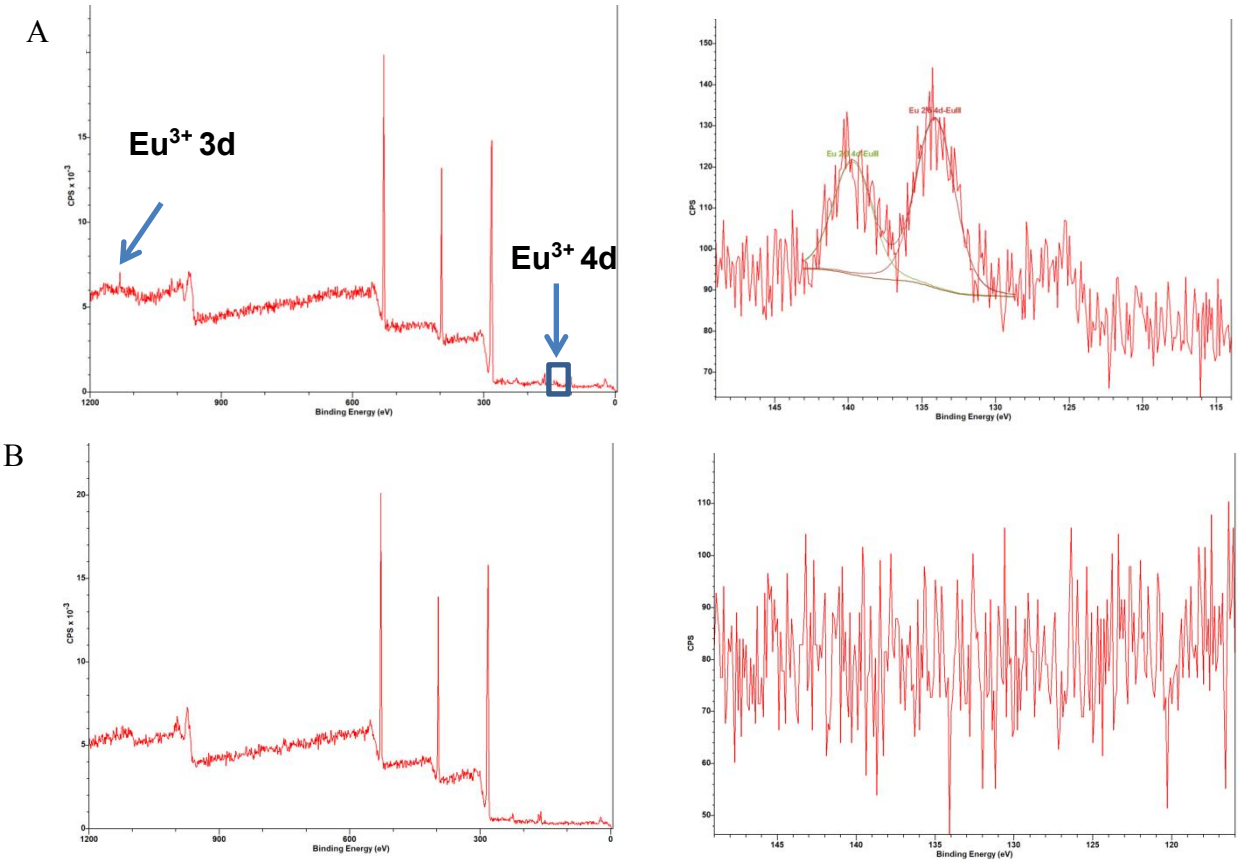

Fig.19. XPS spectra of Eu and high resolution spectra of Eu 4d.
(A)WK-HOPO-MA; (B) WK

Chapter 4. CONCLUSION

In this work, we extracted two types of wool keratin with different mercaptan contents from wool. We used the thiol groups in WK to synthesize silver nanoparticles and a non-natural WK for REEs recovery.

By synthesizing silver nanoparticles under different conditions, we found that the conditions for synthesizing AgNPs with the strongest fluorescence were WK:$AgNO_3$=10mg/ml:5mM, with incubation time and temperature of 23°C and 30min. The fluorescence of these silver NPs is size-dependent.

We have provided preliminary evidence of successful functionalization of wool keratin through changes observed in the CD spectrum and FTIR fingerprint region. Additionally, X-ray photoelectron spectroscopy (XPS) results have confirmed the ability of WK-HOPO-MA to REEs.

To advance our investigation, it is imperative that we verify, through solid state NMR, the successful modification of thiol groups on functionalized WK. Additionally, we can optimize the efficiency of functionalized WK for rare earth element (REE) absorption by regulating the pH value.

REFERENCE

[1] Zoccola M, Aluigi A, Tonin C. Charaterisation of keratin biomass from butchery and wool industry wastes. J Mol Struct 2009; 938: 35–40

[2] Eslahi, N., Dadashian, F., & Nejad, N. H. (2013). An investigation on keratin extraction from wool and feather waste by enzymatic hydrolysis. Preparative biochemistry & biotechnology, 43(7), 624–648..

[3] Shavandi, A., Silva, T. H., Bekhit, A. A., & Bekhit, A. E. A. (2017). Keratin: dissolution, extraction and biomedical application. Biomaterials science, 5(9), 1699–1735.

[4] Moll, R.; Franke, W.W.; Schiller, D.L.; Geiger, B.; Krepler, R. The catalog of human cytokeratins: Patterns of expression in normal epithelia, tumors and cultured cells. Cell 1982, 31, 11−24.

[5] Fraser, R.D.; MacRae, T.P.; Parry, D.A.; Suzuki, E. Intermediate filaments in alpha-keratins. Proc. Natl. Acad. Sci. USA 1986, 83, 1179−1183.

[6] Coulombe, P.A.; Bousquet, O.; Ma, L.; Yamada, S.; Wirtz, D. The 'ins' and 'outs' of intermediate filament organization. Tr. Cell Biol. 2000, 10, 420−428.

[7] Korniłłowicz-Kowalska, T., & Bohacz, J. (2011). Biodegradation of keratin waste: Theory and practical aspects. Waste management (New York, N.Y.), 31(8), 1689–1701.

[8] Jeffrey, P.D. (1972). The molecular weights of the low-sulphur proteins from wool: A review. Journal of the Textile Institute, 63, 91-113.

[9] Shavandi A, Bekhit AE-DA, Carne A, Bekhit A. Evaluation of keratin extraction from wool by chemical methods for bio-polymer application. Journal of Bioactive and Compatible Polymers. 2017;32(2):163-177

[10] Jin, R.. (2010). Quantum sized, thiolate-protected gold nanoclusters. Nanoscale, 2(3), 343–362.

[11] Lu, Y., & Chen, W.. (2012). Sub-nanometre sized metal clusters: from synthetic challenges to the unique property discoveries. Chemical Society Reviews, 41(9), 3594.

[12] Stamplecoskie, K. G., & Kamat, P. V.. (2014). Size-Dependent Excited State Behavior of Glutathione-Capped Gold Clusters and Their Light-Harvesting Capacity. Journal of the American Chemical Society, 136(31), 11093–11099.

[13] Yu, Y., Luo, Z., Chevrier, D. M., Leong, D. T., Zhang, P., Jiang, D.-E., & Xie, J.. (2014). Identification of a Highly Luminescent Au22(SG)18 Nanocluster. Journal of the American Chemical Society, 136(4), 1246–1249.

[14] Zhu, M., Aikens, C. M., Hendrich, M. P., Gupta, R., Qian, H., Schatz, G. C., & Jin, R.. (2009). Reversible Switching of Magnetism in Thiolate-Protected Au25 Superatoms. Journal of the American Chemical Society, 131(7), 2490–2492.

[15] Knoppe, S., Wong, O. A., Malola, S., Häkkinen, H., Bürgi, T., Verbiest, T., & Ackerson, C. J.. (2014). Chiral Phase Transfer and Enantioenrichment of Thiolate-Protected Au102 Clusters. Journal of the American Chemical Society, 136(11), 4129–4132.

[16] Li, G., & Jin, R.. (2014). Gold Nanocluster-Catalyzed Semihydrogenation: A Unique Activation Pathway for Terminal Alkynes. Journal of the American Chemical Society, 136(32), 11347–11354.

[17] Xie, J., Zheng, Y., & Ying, J. Y.. (2009). Protein-Directed Synthesis of Highly Fluorescent Gold Nanoclusters. Journal of the American Chemical Society, 131(3), 888–889.

[18] Yan, L., Cai, Y., Zheng, B., Yuan, H., Guo, Y., Xiao, D., & Choi, M. M. F.. (2012). Microwave-assisted synthesis of BSA-stabilized and HSA-protected gold nanoclusters with red emission. Journal of Materials Chemistry, 22(3), 1000–1005.

[19] Wen, F., Dong, Y., Feng, L., Wang, S., Zhang, S., & Zhang, X.. (2011). Horseradish Peroxidase Functionalized Fluorescent Gold Nanoclusters for Hydrogen Peroxide Sensing. Analytical Chemistry, 83(4), 1193–1196.

[20] Elechiguerra, J. L., Burt, J. L., Morones, J. R., Camacho-Bragado, A., Gao, X., Lara, H. H., & Yacaman, M. J.. (2005). Interaction of silver nanoparticles with HIV-1. Journal of Nanobiotechnology, 3(1), 6.

[21] Bajpai, S. K., Mohan, Y. M., Bajpai, M., Tankhiwale, R., & Thomas, V. (2007). Synthesis of polymer stabilized silver and gold nanostructures. Journal of nanoscience and nanotechnology, 7(9), 2994–3010.

[22] Esumi, K., Suzuki, A., Yamahira, A., Torigoe, K., 2000. Role of poly(amidoamine) dendrimers for preparing nanoparticles of gold, platinum, and silver. Langmuir16, 2604–2608.

[23] Manno, D., Filippo, E., Di Giulio, M., Serra, A., 2008. Synthesis and characterization ofstarch-stabilized Ag nanostructures for sensors applications. J. Non-Cryst. Solids354, 5515–5520.

[24] Zhang, W., Qiao, X., Chen, J., Wang, H., 2006. Preparation of silver nanoparticles inwater-in-oil AOT reverse micelles. J. Colloid Interface Sci. 302, 370–373.X. Lü, S. Cui/Bioresource Technology 101 (2010) 4703–47074707

[25] Raveendran, P., Fu, J., & Wallen, S. L.. (2003). Completely “Green” Synthesis and Stabilization of Metal Nanoparticles. Journal of the American Chemical Society, 125(46), 13940–13941.

[26] Mohan, Y.M., Raju, K.M., Sambasivudu, K., Singh, S., Sreedhar, B., 2007. Preparationof acacia-stabilized silver nanoparticles: a green approach. J. Appl. Polym. Sci.106, 3375–3381.

[27] Govindaraju, K., Basha, S.K., Kumar, V.G., Singaravelu, G., 2008. Silver, gold andbimetallic nanoparticles production using single-cell protein (Spirulinaplatensis) Geitler. J. Mater. Sci. 43, 5115–5122.

[28] Sanghi, R., Verma, P., 2009. Biomimetic synthesis and characterisation of proteincapped silver nanoparticles. Bioresour. Technol. 100, 501–504

[29] Wang, J., Rincon, O., Polsky, R., Dominguez, E., 2003. Electrochemical detection ofDNA hybridization based on DNA-templated assembly of silver cluster.Electrochem. Commun. 5, 83–86

[30] Schrooyen, P.M., Dijkstra, P.J., Oberthur, R.C., Bantjes, A., Feijen, J., 2001.Stabilization of solutions of feather keratins by sodium dodecyl sulfate. J.Colloid Interface Sci. 240, 30–39

[31] Alonso, E., Sherman, A. M., Wallington, T. J., Everson, M. P., Field, F. R., Roth, R., & Kirchain, R. E.. (2012). Evaluating Rare Earth Element Availability: A Case with Revolutionary Demand from Clean Technologies. Environmental Science & Technology, 46(6), 3406–3414.

[32] Cotruvo, J. A., Featherston, E. R., Mattocks, J. A., Ho, J. V., & Laremore, T. N.. (2018). Lanmodulin: A Highly Selective Lanthanide-Binding Protein from a Lanthanide-Utilizing Bacterium. Journal of the American Chemical Society, 140(44), 15056–15061.

[33] Park, D. M., Reed, D. W., Yung, M. C., Eslamimanesh, A., Lencka, M. M., Anderko, A., Fujita, Y., Riman, R. E., Navrotsky, A., & Jiao, Y.. (2016). Bioadsorption of Rare Earth Elements through Cell Surface Display of Lanthanide Binding Tags. Environmental Science & Technology, 50(5), 2735–2742.

[34] Shavandi, A., Silva, T. H., Bekhit, A. A., and Bekhit, A. E.-D. A. (2017b). Keratin: Dissolution, Extraction and Biomedical Application. Biomater. Sci. 5, 1699–1735.

[35] Vasconcelos, A., Freddi, G., and Cavaco-Paulo, A. (2008). Biodegradable Materials Based on Silk Fibroin and Keratin. Biomacromolecules 9, 1299–1305.

[36] Zoccola, M., Aluigi, A., and Tonin, C. (2009). Characterisation of Keratin Biomass from Butchery and Wool Industry Wastes. J. Mol. Struct. 938, 35–40.